

# Early Warning Signals in Mutualistic Population Dynamics

Jordan Snyder, Weiran Cai, Raissa D’Souza

February 28, 2019

## Contents

<b>I</b>	<b>Introduction and Background</b>	<b>2</b>
<b>1</b>	<b>Dynamics on Mutualistic Networks</b>	<b>3</b>
<b>2</b>	<b>Previous work</b>	<b>4</b>
<b>II</b>	<b>Analytical Tools</b>	<b>6</b>
<b>3</b>	<b>Linearization</b>	<b>6</b>
3.1	Non-normality . . . . .	10
<b>4</b>	<b>Linearizing our particular dynamics</b>	<b>11</b>
<b>5</b>	<b>Functional Network Inference and Community Detection</b>	<b>12</b>
<b>III</b>	<b>Simulations and Analysis</b>	<b>14</b>
<b>6</b>	<b>Parameter Setting</b>	<b>14</b>
<b>7</b>	<b>Simulation</b>	<b>15</b>
<b>8</b>	<b>General Observations</b>	<b>15</b>
8.1	Degree Exponent $\delta$ . . . . .	15
8.2	Competition coefficients $\beta$ . . . . .	17
<b>9</b>	<b>Linearization</b>	<b>17</b>
<b>10</b>	<b>Statistics</b>	<b>21</b>
10.1	Spectral Analysis . . . . .	22
10.2	Correlations and Community Structure . . . . .	24

<b>11 Covariance vs. Topology</b>	<b>28</b>
<b>12 Randomizing the Network</b>	<b>30</b>
<b>13 Varying Nestedness</b>	<b>30</b>
<b>14 Histogramology</b>	<b>33</b>
<b>15 Analytical Results</b>	<b>34</b>
15.1 Zero interspecies competition, $\delta = 1$ . . . . .	34
15.2 Uniform Growth Rate . . . . .	36
<b>IV Reframing</b>	<b>40</b>
<b>16 Random network models</b>	<b>40</b>
<b>17 Dynamics</b>	<b>41</b>

### Abstract

This is to record setup and progress on the dynamics and early warning signs side of the mutualistic networks project

## Part I

# Introduction and Background

A *mutualistic network* is one in which there are two *types* or *guilds* of nodes, with the nodes of each guild interacting with the nodes of the other guild in a mutually beneficial way. An archetypal example is the case of plant species and the animal species that pollinate them. Hence we will commonly use the labels  $A$  and  $P$  to denote the two guilds, referring to animals and plants, respectively. We will write  $N_A$  and  $N_P$  to denote the number of nodes (species) in each guild.

One can collect the information of who interacts with whom in the form of a *mutualistic matrix*, which is a  $N_P \times N_A$  matrix whose  $(i, j)^{\text{th}}$  entry indicates the relationship between plant  $i$  and animal  $j$ . There has been extensive study of the structural properties of a mutualistic network that can be read off of this matrix, such as *nestedness* [AP93, BJMO03] and *modularity* [New06, OBDJ07, Bar07].

Modularity is a measurement of the extent to which the links in a network are confined to modules. A typical definition of modularity is of the form

$$Q(\sigma) = \frac{1}{Q_{\text{norm}}} \sum_{i,j} (A_{ij} - \langle A_{ij} \rangle) \delta(\sigma_i, \sigma_j) \quad (1)$$

where  $\sigma$  is a vector defining the partition (i.e.  $\sigma_i$  is the label of the module to which node  $i$  belongs),  $Q_{\text{norm}}$  is a normalization constant ensuring  $Q \leq 1$ ,

and  $\langle A_{ij} \rangle$  is the *expected link weight* between nodes  $i$  and  $j$  under a suitable null model. A typical choice is  $\langle A_{ij} \rangle = k_i k_j / 2m$ , where  $k_i$  is the degree of node  $i$  and  $m = \sum k_i$  is the total number of links. This choice, however, is not appropriate for a bipartite network since it does not respect the constraint that links are always between-guild and never among-guild. The appropriate formulation for bipartite networks was introduced by Barber [Bar07].

Nestedness is a property of a bipartite network that was introduced by Atmar and Patterson in 1993 [AP93]. Their original study system was an ecosystem of separate islands, each inhabited by some collection of species. The bipartite network in this case consists of species in one guild, and islands in the other, with links indicating a given species living on a given island. The fundamental observation of Atmar and Patterson was that the islands inhabited by the rarest species were also inhabited by the more common species; and conversely, that the most sparsely-populated islands contained species that also lived on most or all of the other islands. In network language, the set of neighbors of any given low-degree node is contained within the set of neighbors of any given higher-degree node. It is this "nesting" of neighbor sets that gives us the name "nestedness". Several formulas have been given in attempts to quantify this property, for instance by counting the extent to which neighbor-overlap occurs (NODF) [ANGLU08], or by measuring to what extend nonzero entries in the adjacency matrix are clustered near the top-left corner when columns and rows are sorted by degree (NTC) [AP93].

There has been extensive study of the modularity and nestedness of mutualistic networks. It has been reported that many real mutualistic networks are significantly nested [BJMO03]. The same networks have also been shown to be significantly modular [OBDJ07]. Further work has investigated the origins of these network properties [BFPG<sup>+</sup>09, SRTU09, PHM17].

Our goal will be to study the interplay of the structural properties of the mutualistic networks with dynamics unfolding on them. Therefore we begin by measuring some structural properties of interest for the various Web of Life networks. To do this we use the BiMat software for MATLAB, written by César Flores, Timotheé Poisot, Sergi Valverde, and Joshua Weitz <https://bimat.github.io/>.

[ Insert here a summary of the metastatistics analysis. ]

## 1 Dynamics on Mutualistic Networks

We mention specifically the work of Dakos and Bascompte [DB14], who investigated the relationship between the mutualistic network structure and the warning signs associated with ecosystem collapse. To do this, the authors stud-

ied a toy model of population dynamics, having the form

$$\begin{aligned} dP_i &= P_i \left( \alpha_i^P - \sum_{j=1}^{N_P} \beta_{ij}^P P_j + \frac{\sum_{k=1}^{N_A} \gamma_{ik}^P A_k}{1 + h \sum_{k=1}^{N_A} \gamma_{ik}^P A_k} \right) dt + \sigma P_i dW_{i,t}^P \\ dA_k &= A_k \left( \alpha_k^A - \sum_{l=1}^{N_A} \beta_{kl}^A A_l + \frac{\sum_{i=1}^{N_P} \gamma_{ki}^A P_i}{1 + h \sum_{i=1}^{N_P} \gamma_{ki}^A P_i} \right) dt + \sigma A_k dW_{k,t}^A \end{aligned} \quad (2)$$

where  $P_i$  denotes the abundance of plant species  $i$ ,  $A_k$  the abundance of animal species  $k$ ;  $\alpha^A, \alpha^P$  are vectors of intrinsic growth/death rates;  $\beta^A, \beta^P$  are matrices of intra-guild competition coefficients;  $\gamma^A, \gamma^P$  are mutualistic matrices;  $h$  is a constant known as the handling time, and controls the saturation of the mutualistic term;  $\sigma$  is noise strength; and  $W^A, W^P$  are vectors of standard Brownian motions with independent components.

Given various parameter settings, the authors of [DB14] stress the ecosystem by slowly decreasing the magnitude of the mutualistic coefficients  $\gamma$ , in such a way that total extinction is inevitable. Along the way, it is possible to measure variability in population levels. General considerations imply that one can expect so-called *critical slowing down* in a dynamical system which is brought near a tipping point [SBB<sup>+</sup>09]. Among these are rising variance and autocorrelation in the dynamics.

Indeed, it is found that the coefficient of variation (defined as the standard deviation divided by the mean) and the lag-1 autocorrelation are both significantly larger when the system is close (in terms of the magnitude of  $\gamma$ ) to extinction than when it is far away. These statements hold when the statistical quantities are measured either for the time series of an individual species, or the time series of total ecosystem biomass.

The authors go on to connect the performance of these indicators at the species level to species properties that derive from network position - degree, and contribution to nestedness.

Notice that the early warning indicators just described do not directly illuminate anything about the *mechanism* of ecosystem collapse; they only serve to indicate its proximity. We aim to extend the work of [DB14] by examining pairwise correlations among the biomasses of the various species, with a goal of extracting some narrative understanding of how the ecosystem collapse unfolds.

## 2 Previous work

Here we give background and context for work on the structure of and dynamics on mutualistic networks

- Carlos Gracia-Lázaro, Laura Hernández, Javier Borge-Holthoefer, and Yamir Moreno. The joint influence of competition and mutualism on the biodiversity of mutualistic ecosystems. pages 1–11, mar 2017

- This work studies a population dynamics model that includes both intra-guild competition and inter-guild mutualism. In contrast with previous work, they do not take competition coefficients to be either uniform or randomly distributed, but rather to be related to co-exploitation. That is, species that use the same resources (i.e. other-guild mutualistic partners) are in competition.
- The conclusion is that when competition is structured in the way described above, there is a nontrivial dependence of biodiversity on the competitive and mutualistic strength *together*. Here biodiversity is taken to be the number of species with nonzero population in the steady state.
- This work studies the location of the steady state as a function of network structure / parameters, as opposed to studying the steady state's stability.
- Jacopo Grilli, Tim Rogers, and Stefano Allesina. Modularity and stability in ecological communities. *Nature Communications*, 7(May):1–10, 2016
  - This paper is one of many in the field that formulates a problem in the framework of "generalized modeling". That is, they pose a stability question as a question about the spectrum of a Jacobian matrix. But, rather than actually integrate dynamical equations to find a fixed point at which to compute the Jacobian, they simply posit the form that such a Jacobian must take, and study its properties as a function of various parameter settings determining its entries.

Specifically, the authors consider an underlying random (symmetric) matrix of interaction coefficients, and study the influence of modularity by multiplying this matrix elementwise with the adjacency matrix of a network with a prescribed value of modularity. Hence the relevant parameters are (anti-)modularity, and the mean and variance of interaction coefficients. The authors find that in some cases modularity can have a moderately stabilizing effect, while anti-modularity can have a strongly destabilizing effect

  - The network models considered here are ones with a homogeneous degree distribution
- Paolo Barucca. Localization in covariance matrices of coupled heterogeneous Ornstein-Uhlenbeck processes. *Physical Review E - Statistical, Non-linear, and Soft Matter Physics*, 90(6):1–5, 2014
  - This work gives general considerations about the properties of the eigenvectors of the covariance matrix that arises from a multivariate Ornstein-Uhlenbeck (OU) process. An OU process is simply the name for a linear, time-invariant dynamical system driven by noise, for instance Equation 3.

- The case where the dynamic matrix is diagonal is trivial; the covariance matrix is also diagonal. In this case, the eigenvectors of the covariance matrix are simply the unit vectors; in particular, they are perfectly localized.
  - The author considers a small, symmetric perturbation of a diagonal dynamic matrix, as well as heterogeneous "temperatures" (i.e. squares of noise magnitudes). He then numerically evaluates measures of eigenvector localization as a function of off-diagonal terms and temperatures.
  - Again, this work considers an ensemble of matrices with homogeneous expected degrees.
- Samir Suweis and Paolo D'Odorico. Early warning signs in social-ecological networks. *PLoS ONE*, 9(7), 2014
    - This work proposes a generic measure of critical slowing down, namely the maximum element of the covariance matrix. The authors demonstrate the relationship between this quantity and the real part of the maximum eigenvalue of the Jacobian (one reasonably proxy for "instability"). They find that this relationship depends on the architecture (i.e. mutualistic (++) or antagonistic (-) or parasitic (+-)), the connectance, the degree distribution, and the variance in link strengths.
    - The authors mention the Lyapunov equation as the key relation between the Jacobian and the covariance matrix, and from there perform mainly computational studies. They do include some calculations for the  $2 \times 2$  case, and some more stuff in the SI.

## Part II

# Analytical Tools

### 3 Linearization

Here we do some mathematical analysis that will enable us to interpret the information obtained by measuring correlations between species' abundances. The following mathematical results are not new can be found in, e.g. [Gar96]. What we offer here is a particular interpretation of the result.

In particular, we will calculate the stationary distribution of a stochastic process on a network. To each node  $i \in \{1, \dots, N\}$  we associate a scalar (random) quantity  $X_i$ , which is driven linearly to zero and excited linearly by its neighbors, and subject to external noise. Hence we take a model of the form

$$dX_i = (-r_i X_i + (\mathbf{AX})_i) dt + \sigma_i dW_{i,t} \quad (3)$$

where  $r_i$  indicates the intrinsic stability of  $X_i$ ;  $(AX)_i := \sum_j A_{ij}X_j$  with  $A$  the adjacency matrix of a graph (which we take to be undirected and without self-loops);  $\sigma_i$  is the strength of noise applied to node  $i$  and  $\{W_i\}$  are independent standard Brownian motions.

If we denote by  $p(\mathbf{x}, t)$  the probability density function for  $\mathbf{X}$  at time  $t$ , then  $p$  evolves according to a Fokker-Planck equation

$$\frac{\partial p}{\partial t} = \sum_{i=1}^N -\frac{\partial}{\partial x_i} \left[ \left( -r_i x_i + \sum_{j=1}^N A_{ij} x_j \right) p(\mathbf{x}, t) \right] + \frac{1}{2} \sigma_i^2 \frac{\partial^2}{\partial x_i^2} p(\mathbf{x}, t). \quad (4)$$

We can simplify (Equation 4) by distributing the first partial derivative, and get

$$\frac{\partial p}{\partial t} = \sum_{i=1}^N p(\mathbf{x}, t) r_i - \frac{\partial p}{\partial x_i} \left( -r_i x_i + \sum_{j=1}^N A_{ij} x_j \right) p(\mathbf{x}, t) + \frac{1}{2} \sigma_i^2 \frac{\partial^2}{\partial x_i^2} p(\mathbf{x}, t) \quad (5)$$

Assuming a stationary solution,  $p(\mathbf{x}, t) = p_0(\mathbf{x})$  for all  $t$ , we get  $\frac{\partial p}{\partial t} = 0$ , hence

$$\sum_{i=1}^N \frac{\sigma_i^2}{2} \frac{\partial^2 p_0}{\partial x_i^2}(\mathbf{x}) = \sum_{i=1}^N -p_0(\mathbf{x}) r_i + \frac{\partial p_0}{\partial x_i} \left( -r_i x_i + \sum_{j=1}^N A_{ij} x_j \right). \quad (6)$$

Clearly, this equation is true if it is true term-by-term. Therefore we seek a function  $p_0(\mathbf{x})$  satisfying

$$\frac{\sigma_i^2}{2} \frac{\partial^2 p_0}{\partial x_i^2}(\mathbf{x}) = -p_0(\mathbf{x}) r_i + \frac{\partial p_0}{\partial x_i} \left( -r_i x_i + \sum_{j=1}^N A_{ij} x_j \right), \quad \forall i \quad (7)$$

To find a solution to this equation, we suppose that there is a solution which is a multivariate normal distribution. That is, we suppose that there exists  $\mu \in \mathbb{R}^N$  (the *mean*) and a symmetric, positive definite matrix  $\Sigma \in \mathbb{R}^{N \times N}$  (the *covariance matrix*), such that

$$p_0(\mathbf{x}) = \frac{1}{\sqrt{(2\pi)^N \det(\Sigma)}} \exp \left( -\frac{1}{2} (\mathbf{x} - \mu)^T \Sigma^{-1} (\mathbf{x} - \mu) \right). \quad (8)$$

Here the elements of the matrix  $\Sigma$  are exactly the covariances of the components of  $X$ :

$$\Sigma_{ij} = \langle (X_i - \langle X_i \rangle)(X_j - \langle X_j \rangle) \rangle \quad (9)$$

Since the equations (Equation 7) are linear, we ignore the normalization factor and seek a solution  $p_0(\mathbf{x}) = \exp(-\frac{1}{2}(\mathbf{x} - \mu)^T \Sigma^{-1} (\mathbf{x} - \mu))$ . For convenience we will denote the entries of the matrix  $\Sigma^{-1}$  by  $(s_{ij})$ , and note

$$(\mathbf{x} - \mu)^T \Sigma^{-1} (\mathbf{x} - \mu) = \sum_{j,k} (x_j - \mu_j) s_{jk} (x_k - \mu_k). \quad (10)$$

Moreover,  $\Sigma^{-1}$  will be symmetric because  $\Sigma$  is symmetric. This fact will be used in simplifying the following equations.

First, we calculate all the relevant derivatives of  $p_0$ . We have

$$\begin{aligned}\frac{\partial p_0}{\partial x_i} &= \exp\left(-\frac{1}{2}(\mathbf{x} - \boldsymbol{\mu})^T \Sigma^{-1}(\mathbf{x} - \boldsymbol{\mu})\right) \left(-\frac{1}{2}\right) \left(\sum_{j=1}^N 2s_{ij}(x_j - \mu_j)\right) \\ &= -p_0(\mathbf{x}) \left(\sum_{j=1}^N s_{ij}(x_j - \mu_j)\right).\end{aligned}\quad (11)$$

and then

$$\begin{aligned}\frac{\partial^2 p_0}{\partial x_i^2} &= -\frac{\partial p_0}{\partial x_i} \left(\sum_{j=1}^N s_{ij}(x_j - \mu_j)\right) - p_0(\mathbf{x})s_{ii} \\ &= p_0(\mathbf{x}) \left[\left(\sum_{j=1}^N s_{ij}(x_j - \mu_j)\right)^2 - s_{ii}\right]\end{aligned}\quad (12)$$

We can now insert the partial derivative expressions into (Equation 7). Dropping a common factor of  $p_0(\mathbf{x})$ , we get

$$\frac{\sigma_i^2}{2} \left[ \left(\sum_{j=1}^N s_{ij}(x_j - \mu_j)\right)^2 - s_{ii} \right] = -r_i - \left(\sum_{j=1}^N s_{ij}(x_j - \mu_j)\right) \left(-r_i x_i + \sum_{j=1}^N A_{ij} x_j\right). \quad (13)$$

To solve for  $\mu$  and  $\Sigma^{-1}$  in terms of  $r$  and  $A$ , we compute the coefficients of the  $x_j x_k$  terms on either side of the equation and equate them.

Equating constant terms gives

$$-\frac{\sigma_i^2}{2} s_{ii} = -r_i \implies s_{ii} = \frac{2r_i}{\sigma_i^2}. \quad (14)$$

Equating coefficients of  $x_i$  gives

$$\begin{aligned}\frac{\sigma_i^2}{2} [-2s_{ii}\mu_i] &= -s_{ii}\mu_i r_i \\ -2r_i\mu_i &= -\mu_i r_i \\ \implies \mu_i &= 0.\end{aligned}\quad (15)$$

Hence, we omit writing  $\mu$  in all further calculations.

Next we consider the terms involving  $x_i x_j$ . However, it will turn out that we *cannot*, in general, choose  $(s_{ij})$  to be symmetric and such that the  $x_i x_j$  term vanishes in every individual equation in Equation 7 (in particular, this fails

when the noise strengths are not identical,  $\sigma_i \neq \sigma_j$ ). Hope is not lost, however, because in the *full* equation (Equation 6), both the  $i^{\text{th}}$  and the  $j^{\text{th}}$  component equations contribute an  $x_i x_j$  term. Adding both equations together will let us compute the coefficients of  $x_i x_j$  in the full Equation 6. When we do this, we get

$$s_{ij} (s_{ii}\sigma_i^2 + s_{jj}\sigma_j^2) = s_{ij} (r_i + r_j) + A_{ij}(s_{ii} + s_{jj}) \quad (16)$$

where we have used both that  $s_{ij} = s_{ji}$  and that  $A_{ij} = A_{ji}$ . Further simplification, including using our result for  $s_{ii}$ , yields

$$s_{ij} = -A_{ij} \frac{2\sigma_j^2 r_i + 2\sigma_i^2 r_j}{\sigma_i^2 \sigma_j^2 (r_i + r_j)} \quad (17)$$

In the case that  $\sigma_i = \sigma_j = \sigma$ , this expression simplifies substantially:

$$s_{ij} = \frac{-2A_{ij}}{\sigma^2} \quad (18)$$

which allows us to express the entire matrix as

$$\Sigma^{-1} = \frac{2}{\sigma^2} (\text{diag}(\mathbf{r}) - A) \quad (19)$$

where  $\text{diag}(\mathbf{r})$  denotes the diagonal matrix whose nonzero entries are given by the vector  $\mathbf{r}$ .

If, moreover,  $r_i = r$  for all  $i$ , then we can actually recover the covariance matrix in an interpretable closed form. In this case, we have

$$\begin{aligned} \Sigma^{-1} &= \frac{2}{\sigma^2} (r\mathbf{I} - A) \\ \Sigma &= \frac{\sigma^2}{2} (r\mathbf{I} - A)^{-1} \\ &= \frac{\sigma^2}{2r} \sum_{k=0}^{\infty} \left( \frac{A}{r} \right)^k \end{aligned} \quad (20)$$

which is the Neumann series for the resolvent of a matrix. Clearly, this expression only converges when  $r$  is larger, in absolute value, than the largest eigenvalue of  $A$ . In view of the dynamics, Equation 3, this is precisely the condition that guarantees that  $\mathbf{x} = 0$  is a stable fixed point of the deterministic dynamics. If this condition is violated, then certainly there is no stationary density that is multivariate normal about zero.

Finally, we can glean some insight from this form of  $\Sigma$ . It is not hard to show that the  $(i, j)^{\text{th}}$  entry of  $A^k$  is a sum over paths from node  $i$  to node  $j$  of the product of edge weights along the path. If  $A_{ij} \in \{0, 1\}$ , then the product along any path is just 1, and  $(A^k)_{ij}$  simply counts the paths.

So, Equation 20 suggests an interpretation of covariance as a quantity that is transmitted by links and damped by nodes. We can conclude, as we might have guessed, that pairs of nodes between which there are many short paths will

co-vary strongly, while nodes connected by only a few long paths will be closer to independent.

Finally, we point out that there is a general, closed-form formula for  $\Sigma$  in terms of the dynamical matrix  $A$  and the noise matrix  $B$ . Noting that the stationary solution is

$$X = \int_0^\infty \exp(tA)BdW_t \quad (21)$$

we obtain [Gar96]

$$\Sigma = \langle XX^T \rangle = \int_0^\infty \exp(tA)BB^T \exp(tA^T)dt \quad (22)$$

If we assume that  $A$  can be (not necessarily orthogonally) diagonalized, then we can write  $A = V\Lambda V^{-1}$ , where  $V$  is the matrix whose columns are eigenvectors of  $A$ , and  $\Lambda$  is the matrix with the eigenvalues of  $A$  on the diagonal. Inserting this form into Equation 22 yields

$$\Sigma = V \left[ \int_0^\infty e^{\Lambda t} V^{-1} BB^T V e^{\Lambda t} dt \right] V^{-1}. \quad (23)$$

We can interpret Equation 23 in the following way: the term in square brackets is the matrix of  $\Sigma$  expressed in the  $V$  basis. Conversely, the term  $V^{-1}BB^TV$  is the matrix of  $BB^T$  in the canonical basis, if the  $BB^T$  is considered to be expressed in the eigenbasis  $V$ . This is horribly confusingly stated, and I'm fairly sorry. Not too sorry, just a little bit.

### 3.1 Non-normality

Unfortunately, much of the above discussion is not terribly applicable due to the severity of the assumption that the matrix defining the dynamics is normal. A sufficient condition for normality is symmetry - in network language, this means that the underlying graph is undirected. Generically, a directed graph will have a non-normal adjacency matrix. This can lead to some surprising results, as we now demonstrate.

Perhaps the simplest example of a non-normal matrix is the  $2 \times 2$  Jordan block:

$$A = \begin{bmatrix} 1 & 1 \\ 0 & 1 \end{bmatrix} \quad (24)$$

We now consider the SDE  $dX = -AXdt + \sigma IdW(t)$ . In components, this is

$$dx_1 = -(x_1 + x_2)dt + \sigma dW_1(t) \quad (25)$$

$$dx_2 = -x_2dt + \sigma dW_2(t) \quad (26)$$

Clearly, the deterministic part of the dynamics ( $dX/dt = -AX$ ) has a unique fixed point at the origin, and this fixed point is stable since all singular values of  $-A$  have negative real part.

The covariance matrix  $\Sigma$  in the stationary state satisfies the equation [Gar96]

$$A\Sigma + \Sigma A^T = \sigma^2 I \quad (27)$$

We can simply solve by hand for the components of  $\Sigma$  and get

$$\Sigma = \sigma^2 \begin{bmatrix} 3/4 & -1/4 \\ -1/4 & 1/2 \end{bmatrix} \quad (28)$$

## 4 Linearizing our particular dynamics

Here we record the calculation of the Jacobian of the (deterministic part of the) dynamics Equation 2.

Since there are two guilds, we need to compute terms of four types:  $\partial\dot{P}_i/\partial P_j$ ,  $\partial\dot{P}_i/\partial A_k$ ,  $\partial\dot{A}_k/\partial P_i$ , and  $\partial\dot{A}_k/\partial A_l$ . With deepest apologies to the Gods of indexing conventions, we have

$$\frac{\partial\dot{P}_i}{\partial P_m} = (1 - \delta_{im}) [-\beta_{im}^P P_i] + \delta_{im} \left[ \alpha_i^P - \sum_{j=1}^{N_P} \beta_{ij}^P P_j + \frac{\sum_{k=1}^{N_A} \gamma_{ik}^P A_k}{1 + h \sum_{k=1}^{N_A} \gamma_{ik}^P A_k} - \beta_{ii}^P P_i \right] \quad (29)$$

$$\frac{\partial\dot{A}_k}{\partial A_n} = (1 - \delta_{kn}) [-\beta_{kn}^A A_k] + \delta_{kn} \left[ \alpha_k^A - \sum_{l=1}^{N_A} \beta_{kl}^A A_l + \frac{\sum_{j=1}^{N_P} \gamma_{kj}^A P_j}{1 + h \sum_{j=1}^{N_P} \gamma_{kj}^A P_j} - \beta_{kk}^A A_k \right] \quad (30)$$

$$\frac{\partial\dot{P}_i}{\partial A_l} = \frac{P_i}{\left(1 + h \sum_{k=1}^{N_A} \gamma_{ik}^P A_k\right)^2} \gamma_{il}^P \quad (31)$$

$$\frac{\partial\dot{A}_k}{\partial P_j} = \frac{A_k}{\left(1 + h \sum_{i=1}^{N_P} \gamma_{ki}^A P_i\right)^2} \gamma_{kj}^A \quad (32)$$

Notice that, sadly, the Jacobian matrix is not symmetric:  $\partial\dot{P}/\partial A \neq (\partial\dot{A}/\partial P)^T$ . Moreover, we should not expect the Jacobian to be normal (i.e. to commute with its transpose), and so the arguments in section 3 should be carefully modified.

In the end we will use this Jacobian to evaluate stability of a fixed point, and to compute and interpret covariances between variables in the vicinity of a fixed point.

Using this Jacobian, we can plug it into Equation 22 to see what analytical relationship we can derive between the mutualistic interaction matrix and the covariance matrix. First, some assumptions. We assume that all growth rates are equal ( $\alpha_i = \alpha \forall i$ ); that  $\delta = 1$ , that is, mutualistic interaction strength is

inversely proportional to in-degree; and that inter-species competition  $\beta_{ij}^G = N_G^{-1}$  for  $G \in \{A, P\}, i \neq j$  while intra-species competition is unity. These assumptions taken together imply that for certain parameter ranges, there exists a fixed point solution in which all abundances are equal and have value  $x \in \mathbb{R}$ . In this case, the noise matrix is  $B = \sigma x I$ . Then Equation 22 becomes

$$\Sigma = \sigma x \int_0^\infty e^{Jt} e^{J^T t} dt \quad (33)$$

If it were the case that  $JJ^T = J^T J$ , then it would hold that  $\exp(Jt) \exp(J^T t) = \exp((J + J^T)t)$ , and we could write a closed-form expression for  $\Sigma$ , which would agree with Equation 20. Without this assumption, however, we must turn to other methods to understand the integral.

Integration by parts applies; we get

$$\Sigma = \sigma x \left( J^{-1} e^{Jt} e^{J^T t} \Big|_0^\infty - \int_0^\infty J^{-1} e^{Jt} J^T e^{J^T t} dt \right) \quad (34)$$

$$= \sigma x \left( -J^{-1} - \int_0^\infty J^{-1} e^{Jt} J^T e^{J^T t} dt \right) \quad (35)$$

We can keep integrating by parts, generating a series of powers of  $J^{-1}$  with alternating signs, but there is no guarantee that this series will converge.

## 5 Functional Network Inference and Community Detection

Here we discuss general aspects of the problem of inferring an effective interaction structure (i.e. a *functional network*) from multiple time series. This problem has been studied extensively, largely in the context of economics and neuroscience.

To narrow the scope somewhat, note that it is reasonable to expect that our system of study, Equation 2, will be near a stable equilibrium point, and that a linear approximation will be appropriate. As shown in section 3, this means that the dependencies between variables will be entirely captured by *covariance* - that is, there will be no (or rather, insignificant) nonlinear dependencies. For this reason, we restrict our attention to analysis of covariance (and/or correlation) matrices.

It is tempting to simply compute a correlation matrix, interpret its entries as weighted edges of a network, and apply an out-of-the-box community detection algorithm to infer functional communities. However, this approach shows a bias - in particular, it will systematically under-detect large communities [MG13].

An approach that has been used in the field of "econophysics" is based on spectral analysis of correlation matrices and random matrix theory. Briefly, the method works as follows (adapted from [MG13]):

Let  $C \in [-1, 1]^{N \times N}$  be an empirical correlation matrix, that is, a matrix of correlations computed from  $L$  samples of  $N$  random variables. Our goal will be to extract features of  $C$  that differ from what would be expected by chance, i.e. what is expected under an appropriate null model. Here the null model is the model in which all  $N$  random variables are, in fact, uncorrelated, and so any nonzero off-diagonal entries in  $C$  would be due to finite sample effects.

We should then specify how to compare our empirical  $C$  to the null model. This comparison should respect the overall structure of the matrix, not just the magnitudes of its various entries. This indicates that we should use a spectral decomposition. And indeed, the expectation of the null model is given in a very precise form by results of random matrix theory (RMT). In particular, the eigenvalues of a correlation matrix computed from  $L$  samples of each of  $N$  uncorrelated random variables will be distributed according the Marcenko-Pastur density  $\rho(\lambda)$  given by

$$\rho(\lambda) = \frac{L}{N} \frac{\sqrt{(\lambda - \lambda_-)(\lambda_+ - \lambda)}}{2\pi\lambda} \text{ if } \lambda_- \leq \lambda \leq \lambda_+ \quad (36)$$

where

$$\lambda_{\pm} = \left[ 1 \pm \sqrt{\frac{N}{L}} \right]^2 \quad (37)$$

Since  $C$  is symmetric, it can be diagonalized:  $C = \sum_{\lambda \in \sigma(C)} \lambda P_{\lambda}$ , where all  $\lambda$  are real eigenvalues and  $P_{\lambda}$  is the projector onto the eigenspace corresponding to eigenvalue  $\lambda$ . The RMT result then gives a natural distinction between eigenvalues that we could expect by finite-sample effects and eigenvalues that reflect some non-trivial relationship among the variables.

In econophysics, it is typical to break  $C$  up into three pieces,  $C = C^{(r)} + C^{(g)} + C^{(m)}$ , corresponding to "random", "group", and "market" modes, respectively. These pieces are defined as

$$C^{(r)} = \sum_{\lambda \leq \lambda_+} \lambda P_{\lambda} \quad (38)$$

$$C^{(g)} = \sum_{\lambda_+ < \lambda < \lambda_m} \lambda P_{\lambda} \quad (39)$$

$$C^{(m)} = \lambda_m P_{\lambda_m} \quad (40)$$

where  $\lambda_m$  denotes the largest eigenvalue of  $C$ . The typical interpretation is that  $C^{(m)}$  reflects any global correlations among the  $N$  variables, while  $C^{(g)}$  represents correlations among some, but not all, of the variables. One can also group these two together as a "structured" component,  $C^{(s)} = C^{(g)} + C^{(m)}$ .

The authors of [MG13] go on to propose three candidate definitions of modularity, based on the above considerations, to use as a basis for community

detection in correlation matrices. A *general* modularity function has the form

$$Q(\vec{\sigma}) = \frac{1}{A_{\text{norm}}} \sum_{i=1}^N (A_{ij} - \langle A_{ij} \rangle) \delta(\sigma_i, \sigma_j) \quad (41)$$

where  $\langle A_{ij} \rangle$  is an expected value of matrix entry  $A_{ij}$  under some null model and  $A_{\text{norm}}$  is a normalization constant.

In consideration of the RMT results above, [MG13] proposes either

- (i)  $\langle C_{ij} \rangle^{(1)} = \delta_{ij}$
- (ii)  $\langle C_{ij} \rangle^{(2)} = C_{ij}^{(r)}$
- (iii)  $\langle C_{ij} \rangle^{(3)} = C_{ij}^{(r)} + C_{ij}^{(m)}$

Inserting any of these three expressions in the definition for modularity gives a quality function that can be maximized by an algorithm of one's choosing.

## Part III

# Simulations and Analysis

Here we describe the computational studies we have performed of the system (Equation 2).

## 6 Parameter Setting

Here we describe the procedures for choosing parameter values - particularly  $\gamma^A, \gamma^P, \beta^A, \beta^P$ . Following [DB14], we generate the mutualistic matrices  $\gamma$  from empirical data collated in the Web of Life database (<http://www.web-of-life.es>). This database contains data from several different ecosystems. For each ecosystem, the data is presented as a matrix with rows indexed by plant species and columns indexed by pollinator species. The matrix entries (either binary or weighted) indicate the interactions between the corresponding species.

To generate a tunable family of mutualistic matrices, we take coefficient values to be

$$\gamma_{ij} = \gamma_0 \frac{y_{ij}}{k_i^\delta} \quad (42)$$

where  $\{y_{ij}\}$  are the raw interaction values from the database,  $\gamma_0$  is an overall scale factor,  $k_i = \sum_j y_{ij}$  is the (weighted) in-degree of node  $i$ , and  $\delta \in [0, 1]$  is an exponent that quantifies a trade-off between generality and mutualistic benefit. If  $\delta = 0$ , then each mutualistic partner of species  $i$  confers the same amount of benefit. If  $\delta > 0$ , then the mutualistic benefit conferred by each partner decreases as the total number of partners decreases. In the extreme

case of  $\delta = 1$ , we have  $\sum_j \gamma_{ij} = \gamma_0$  for all  $i$ , so the total mutualistic benefit for every species is the same.

For the competition coefficients, we set all  $\beta_{ii} = 1$  and sample  $\beta_{ij}$  randomly from a uniform distribution with minimum 0.001 and mean  $1/n$ , where  $n$  is the number of species in the respective guild (plants or animals). This is rather arbitrary and completely copied from [DB14]; we also consider the case of very small (or zero) interspecific competition. As it turns out, the results are remarkably different.

The intrinsic growth rates  $\alpha$  are also chosen at random. In fact, "growth rate" is a somewhat misleading name, because they are chosen from a uniform distribution on  $[-0.5, -0.1]$ . This is so that there can be no survival when mutualistic strength  $\gamma_0$  is brought to zero, and we know that every simulation of such a situation will result in total extinction.

## 7 Simulation

Following [DB14], we generate sample paths of the solution to Equation 2 using an Euler-Maruyama scheme with a time step of  $\delta t = 0.01$ . In practice, we record all species abundances in a single vector  $X = (P^T, A^T)^T$ . In other words,  $X_i = P_i$  for  $i \in 1 \dots N_P$ , and  $X_i = A_{i-N_P}$  for  $i \in N_P \dots N_P + N_A$ .

## 8 General Observations

Here we list some general observations about the behavior of Equation 2 as it depends on the various parameter settings.

### 8.1 Degree Exponent $\delta$

The parameter  $\delta$ , as it appears in Equation 42, has a very strong effect on nature of the dynamics, particularly in the approach to ecosystem collapse. The main differences are displayed in Figure 1.

If  $\delta = 1$ , then the sum of the incoming mutualistic coefficients to each species is constant. This puts all species on roughly "equal footing", and so a global decrease in mutualistic strength (i.e. a decrease in  $\gamma_0$ ) will affect all species in a similar manner. This is the case until some species goes completely extinct, at which point imbalances appear, and the subsequent dynamics towards total extinction are much more erratic.

If, on the other hand,  $\delta = 0$ , then each mutualistic interaction has the same strength. In this way, generalist species (those with many mutualistic partners) stand to benefit much more than specialists (those with few mutualistic partners). This naturally creates a variation in terms of the response of the various population levels to a global decrease in mutualistic strength.

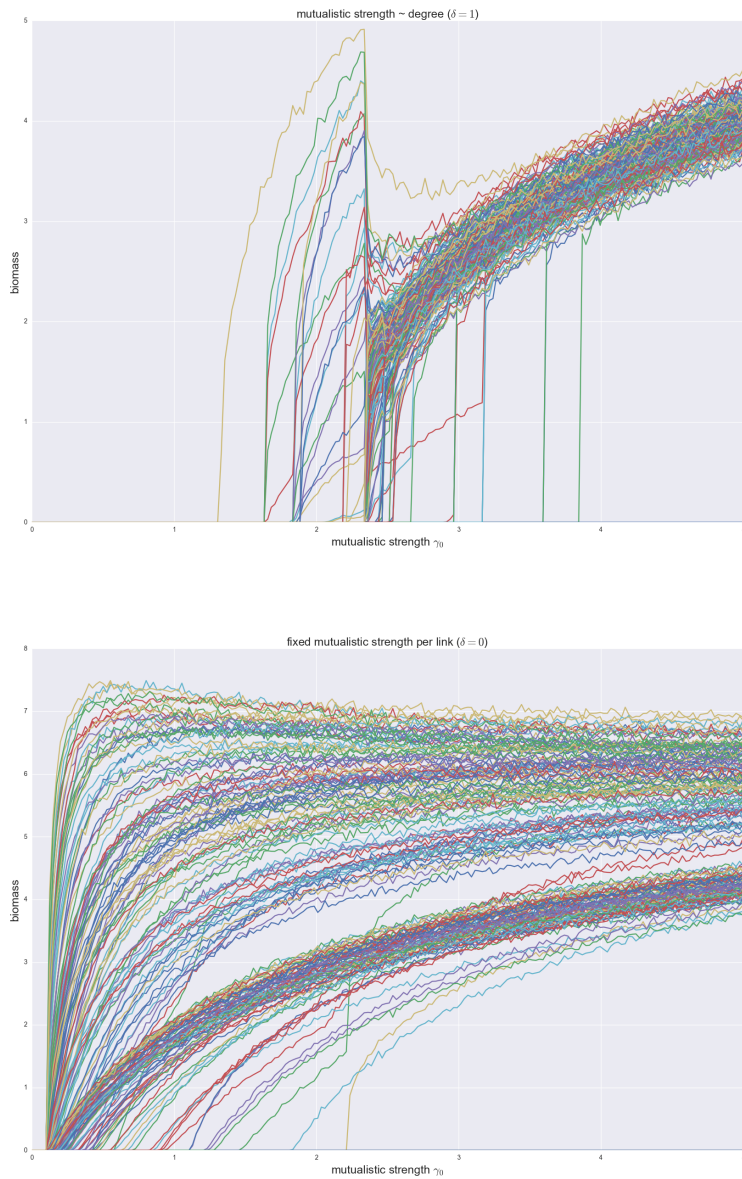


Figure 1: Effect of degree exponent  $\delta$ . Data are species abundances generated by slowly decreasing  $\gamma_0$  to zero.

## 8.2 Competition coefficients $\beta$

The size and the heterogeneity of the competition coefficients  $\{\beta_{ij}^A, \beta_{ij}^P\}$  also has a strong effect on the dynamics. A visual summary is given in Figure 2

To guide intuition, consider the extreme case of zero competition between species. In this case, the only interactions between species are positive ones. If the strength of these connections decreases, then so will the abundances of all species. If one species goes extinct, then its mutualistic partners will be impacted negatively, as will the partners of those partners, and so on. This gives rise to a tendency for different species to go extinct together. If we *also* have  $\delta = 1$ , then this effect is especially pronounced, since in this case all species have equal incoming mutualistic strengths.

If, however, there is significant competition among species, then one species going extinct may represent a benefit for a competitor species! Indeed, we can see this effect prominently in both parts of Figure 1, though more strongly in the  $\delta = 1$  case.

## 9 Linearization

Based on intuition from the exactly-solvable two-species version of our model (see [DB14] Supplementary Information), we expect species extinction to occur as a saddle-node bifurcation, and therefore we expect the dominant eigenvalue of the Jacobian to approach zero. Indeed, this is what we see, Figure 3.

We can go further than just the eigenvalue, and examine the corresponding eigenvector(s). Since the Jacobian is not generally symmetric (or even normal), the eigenvalue decomposition yields both left and right eigenvectors; that is, there are matrices  $V, D, W$  such that  $D$  is the diagonal matrix of eigenvalues and  $AV = DV$  and  $W^T A = DW^T$ , so that the columns of  $V$  are right eigenvectors of  $A$  and the columns of  $W$  are left eigenvectors of  $A$ . We focus on the right eigenvectors  $V$  since these correspond to directions such that a perturbation in that direction will decay along that direction at a rate given by the appropriate eigenvalue.

In the first extinction event in this experiment, the species numbered 36 and 177 go extinct together. We can see this fact reflected in the right eigenvector corresponding to the eigenvalue which is closest to zero in the step immediately before these two species go extinct, see Figure 4.

We wish to connect this localization phenomenon in the critical Jacobian mode to properties of the covariance matrix. As stated before section 3, the Jacobian  $J$  and covariance matrix  $\Sigma$  enjoy the relationship

$$-J\Sigma - \Sigma J^T = BB^T \quad (43)$$

provided the system is well-approximated by local linearization, where  $B$  is the matrix by which noise is injected. In this case, since we have multiplicative noise,  $B$  is a diagonal matrix whose entries are  $(\sigma X_i)$ , where  $\sigma \in \mathbb{R}$  is the overall noise strength and  $\{X_i\}$  are the species abundances.

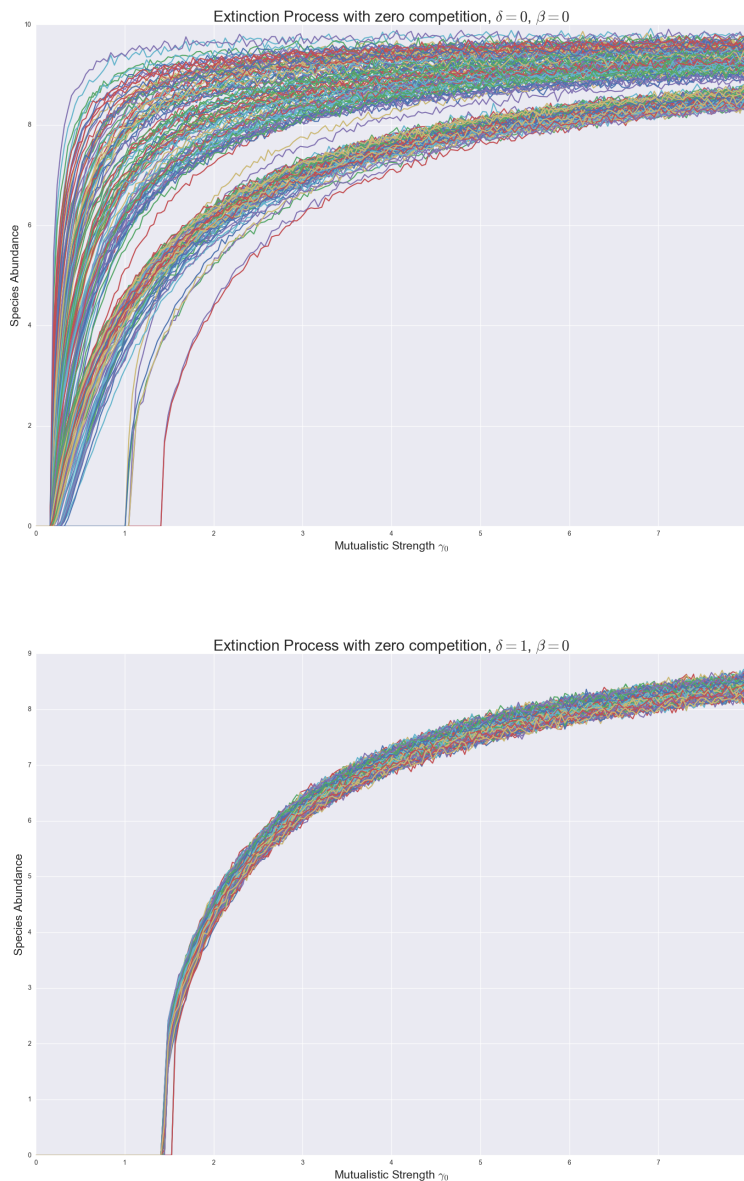


Figure 2: Extinction process in the absence of interspecies competition. Note that abundances decrease monotonically to zero (up to small fluctuations due to noise)

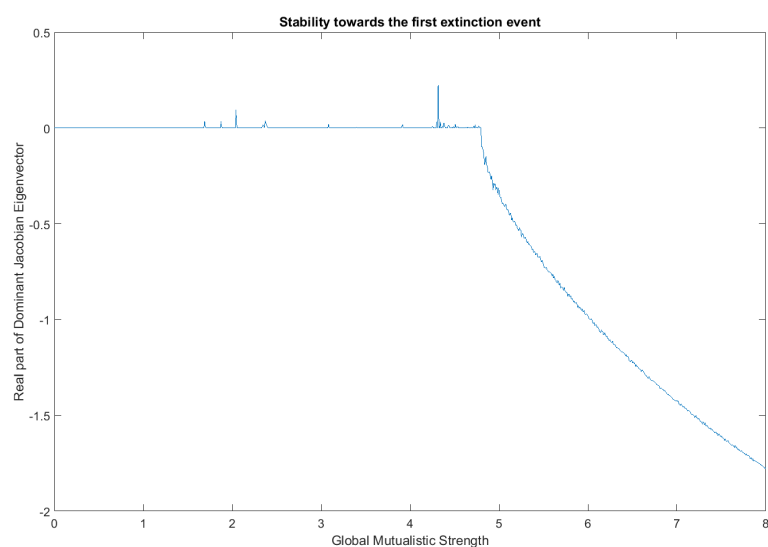


Figure 3: The largest (real part of an) eigenvalue of the Jacobian as a function of mutualistic strength. Mutualistic strength  $\gamma_0$  was decreased in 1000 equal-sized steps from 8 to 0, and for each value of  $\gamma_0$  the dynamics were simulated until the mean abundance of each species was reasonably stationary. The system state used for calculation of the Jacobian matrix was the vector of mean abundances for all species over the last (stationary) integration time period.

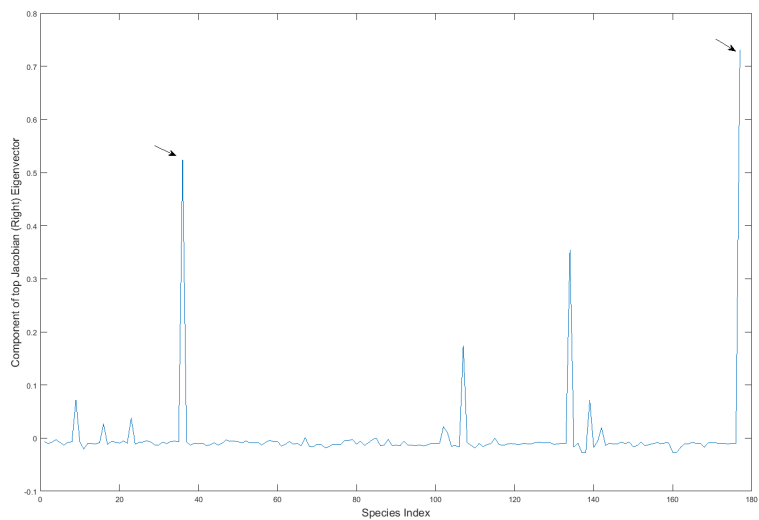


Figure 4: The right eigenvector corresponding to the eigenvalue nearest to zero immediately preceding the first extinction event. In this extinction event, species 36 and 177 go extinct; their entries in this eigenvector are clearly the largest, as indicated by the arrows. In other words, the critical mode is concentrated on the most vulnerable species, which aligns with our intuition from low-dimensional saddle-node bifurcations.

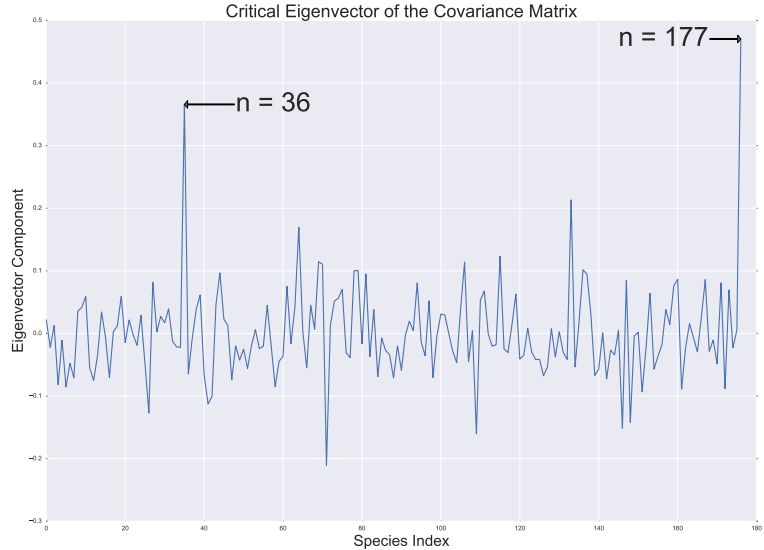


Figure 5: The leading (largest eigenvalue) eigenvector of the covariance matrix immediately preceding the first extinction event, in which species 36 and 177 go extinct. As for the leading Jacobian eigenvector, the two species that are about to go extinct are those whose components in this vector are largest.

Intuitively, as the system approaches a tipping point, abundances remain reasonably large, and the  $B$  matrix is roughly constant; in particular, it remains full rank. However,  $J$  has an eigenvalue tending to zero, bringing it closer to being rank-deficient. Therefore we expect that  $\Sigma$  will develop a mode with a large eigenvalue so that Equation 43 remains satisfied. As we have seen, the critical mode of the Jacobian displays readily interpretable information about the impending extinction event; this also appears to be the case for the top eigenvector of the covariance matrix, see Figure 5.

## 10 Statistics

We investigate several statistical quantities of interest from sampled trajectories  $X(t)$ . In what follows, angle brackets denote, in principle, statistical averages - that is, averages over an ensemble of sample paths. In practice, however, we assume that the process  $X$  is stationary and ergodic, meaning that we can estimate these averages by averages over time. First, the coefficient of variation,

defined as the standard deviation divided by the mean:

$$CV_i = \frac{\sqrt{\langle (X_i - \langle X_i \rangle)^2 \rangle}}{\langle X_i \rangle}. \quad (44)$$

This quantity is an appropriate substitute for the standard deviation in the present context because the system (2) is subject to multiplicative noise (i.e. the noise strength is proportional to the abundance). We can also consider the coefficient of variation at the community level, by replacing  $X_i$  by  $\sum_i X_i$  in the above definition.

Next, we consider the lagged correlations:

$$C_{ij}(\tau) = \frac{\langle (X_i(t + \tau) - \langle X_i \rangle)(X_j(t) - \langle X_j \rangle) \rangle}{\sigma_i \sigma_j} \quad (45)$$

where we caution that here  $\sigma_i$  and  $\sigma_j$  are the standard deviations of variables  $X_i$  and  $X_j$ , respectively, rather than the noise strengths as written in (Equation 2). The correlation  $C_{ij}(\tau)$  takes values in  $[-1, 1]$ , and measures the degree to which the value of  $X_j$  at time  $t$  predicts the value of  $X_i$  at time  $t + \tau$ .

The dependence of  $C_{ij}(\tau)$  on the lag  $\tau$  can tell us about the nature of the connection between species  $i$  and  $j$ . In particular, the diagonal terms  $C_{ii}(\tau)$  can give a characteristic timescale for the *autocorrelation* of species  $i$ . Empirically (see Figure 6), we find that each diagonal element depends nearly exponentially on  $\tau$ , that is

$$C_{ii}(\tau) \approx \exp(-\tau/T_i) \quad (46)$$

for some  $T_i$ , which gives a characteristic timescale for the fluctuations in the abundance of species  $i$ .

## 10.1 Spectral Analysis

Here we perform some simple spectral analyses of correlation matrices obtained along the course towards extinction. The discussion in section 5 suggests that we may stand to learn a lot from simply studying the largest eigenvalue of the covariance (and/or correlation) matrix.

Indeed, the spectrum of the correlation matrix is highly sensitive to the dynamics. For example, see Figure 7. This figure was obtained by integrating the dynamics to steady state and calculating the matrix of correlations between species abundances, then changing the overall mutualistic strength and repeating the process. Given these matrices, we computed all eigenvalues (of which there are  $N = 185$ , equal to the total number of species), and plotted a histogram of their values. This histogram can then be compared to the distribution one would expect from measuring a matrix of correlations between uncorrelated random variables, the Marcenko-Pastur distribution.

The first pane of the figure is taken at  $\gamma_0 = 8$ , which is quite far from any extinction event. Note that the distribution of eigenvalues is somewhat wide, but its width is still within an order of magnitude of the width of the

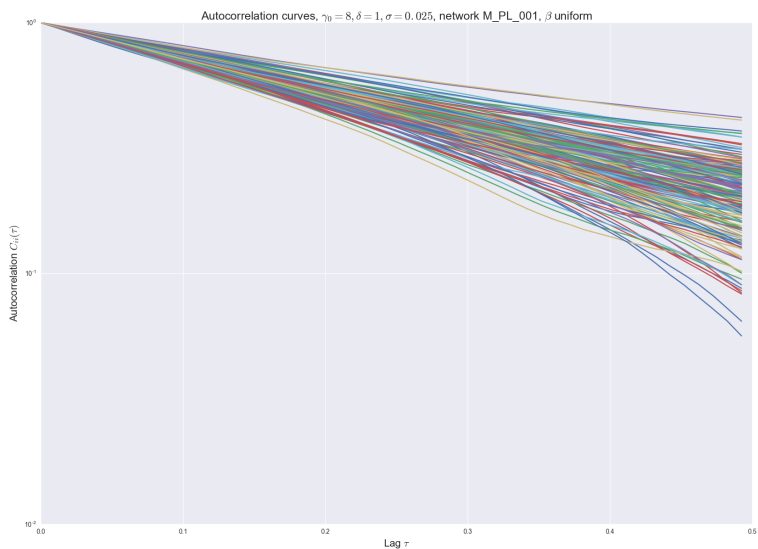


Figure 6: Log-linear plot of single-species autocorrelation curves. Notice each curve is nearly linear, indicating a nearly exponential decay of autocorrelation. The inverse of the slope gives a natural timescale for fluctuations of each species.

Marcenko-Pastur distribution, shown in green. The second pane, however, is taken at  $\gamma_0 = 4$ , which is much closer to an extinction event. We see in this case that while many eigenvalues are still on the order of the level expected at random, the top eigenvalue is much larger.

**NOTE:** These statistics were computed improperly. That is, it was not checked whether or not the dynamics had reached a steady state before calculating correlations. The upshot is that any pair of species that went extinct in the same time window are perceived to be (artificially) highly correlated, since they both exhibit a strong downward trend in abundance.

Given this observation, as well as the computation in section 3, we may expect the correlation matrix to show a very large largest eigenvalue preceding extinction events. Indeed, the calculation in section 3 shows that, in a certain special case, the covariance matrix is inverse to the Jacobian matrix. If an eigenvalue of the Jacobian matrix approaches zero, as one might expect in the vicinity of a saddle-node bifurcation, then the covariance matrix will show a corresponding divergent eigenvalue.

We can test this prediction computationally; at each value of  $\gamma_0$  along the way from high (8) to low (0), we compute the top eigenvalue of both the correlation matrix and the covariance matrix, and plot them as a function of  $\gamma_0$ . We also place vertical lines at the values of  $\gamma_0$  at which extinction events were observed. The results are shown in Figure 8.

As we can see in Figure 8, there are subtle differences between the top eigenvalue of the correlation matrix versus the covariance matrix. Since the correlation matrix is obtained by dividing the covariance matrix by the appropriate standard deviations, the correlation matrix is sensitive to small value of standard deviations. Note that once a species goes extinct, its standard deviation (as well as its covariance with other species) drops to zero, so the rows and columns corresponding to extinct species in the correlation matrix are subject to numerical error to a greater extent than the same rows and columns in the covariance matrix.

## 10.2 Correlations and Community Structure

Here we report observations of the structure of the correlation matrix as it relates to the structure of the mutualistic network  $\gamma$ .

The intuition is that if the mutualistic network is modular (which is the case for some, but not all, of the data sets in the Web of Life), then nodes in the same module should be more highly correlated than nodes in different modules.

To validate this intuition, we measure the correlation matrices as described above, and sort their rows and columns according to a modularity-maximizing partition of the structural network. An example of such a matrix is visualized in Figure 9.

We can go further and watch the evolution of this steady-state correlation matrix as the mutualistic strength  $\gamma_0$  is decreased down to zero. As we expect,

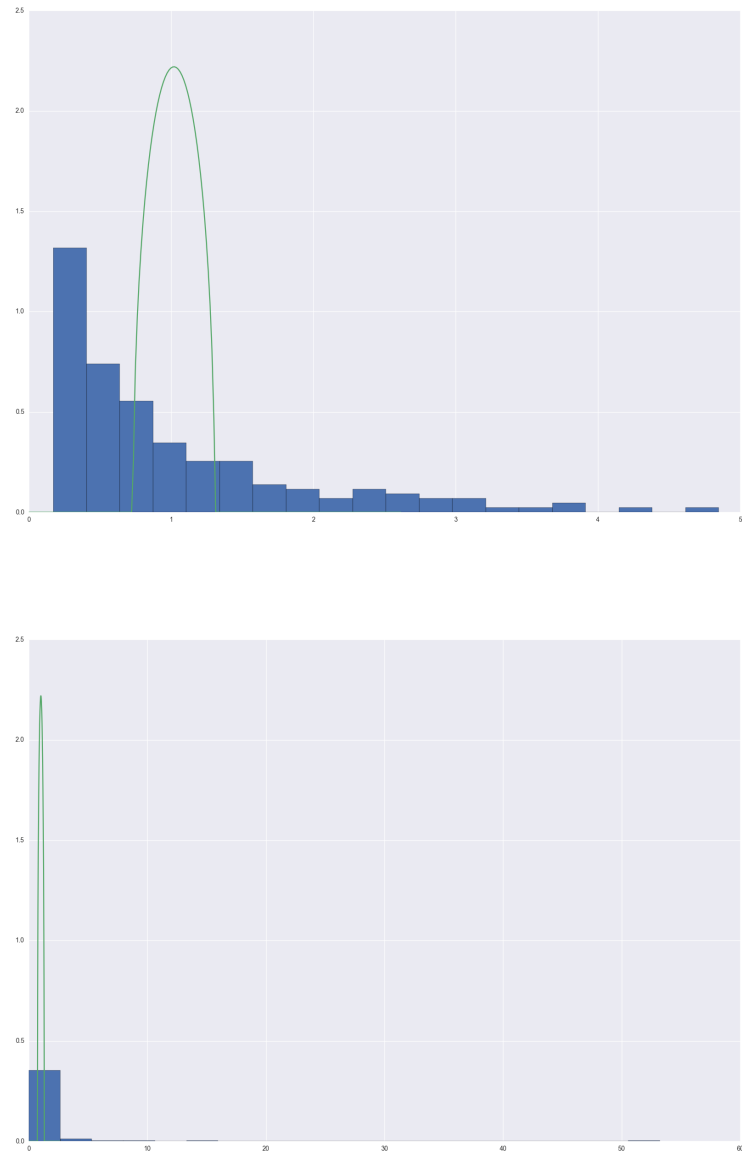


Figure 7: Distribution of eigenvalues of the correlation matrix computed for species abundances around steady state far from the tipping point (top) and close to the tipping point (bottom). In both figures, the green curve is the density of the appropriate Marcenko-Pastur distribution, which gives the expected behavior under the assumption of no actual correlation. Note that the horizontal axes have different scales.

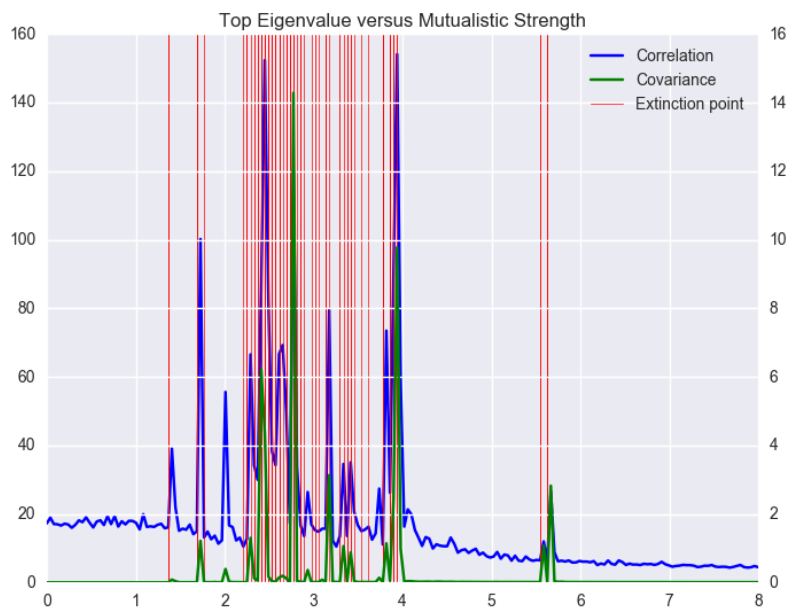


Figure 8: Top eigenvalue of each of the correlation matrix and covariance matrix, computed in steady state, as a function of mutualistic strength. Vertical red lines indicate extinction events.

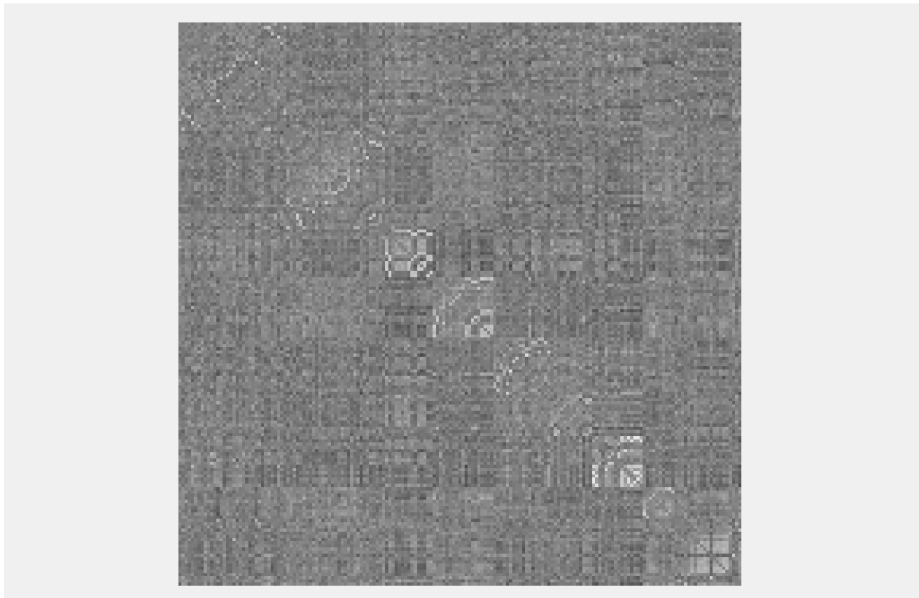


Figure 9: A (equal-time) correlation matrix of species abundances, immediately preceding the first extinction event. Values are indicated by shade, with black representing -1 and white representing +1. Rows and columns are sorted according to a partition of the mutualistic network into  $M = 9$  modules. Visually, there appears to be a block-like structure; that is, correlation appears to respect the modularity of the mutualistic network.

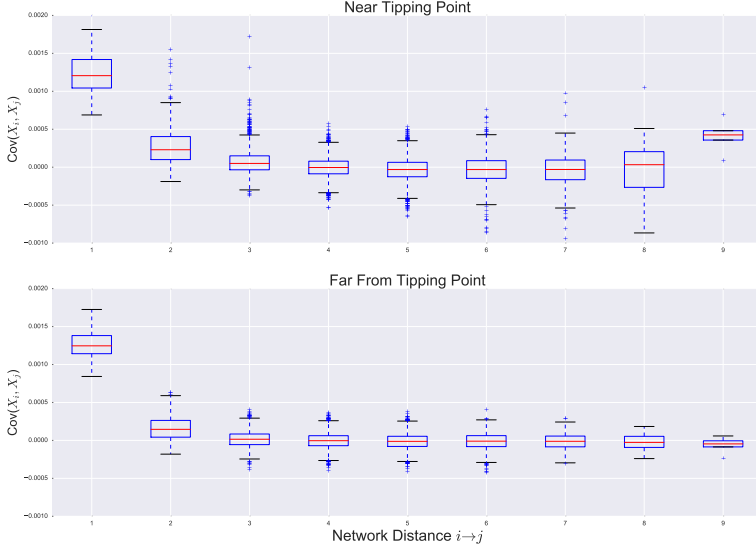


Figure 10: Boxplot of covariance values at different network distances, both near to and far from the tipping point. Each pair of nodes is a data point. Box shows upper and lower quartiles, red line is the median, and whiskers extend to extreme values. Note: overall decrease of covariance with network distance, though decay of covariance with distance appears slower when the system is near the tipping point than when the system is far from the tipping point.

we see increased correlation prior to extinction among sets of species that go extinct in the same step of  $\gamma_0$ .

## 11 Covariance vs. Topology

Here we discuss observations of the relationship between the covariance between any given pair of species  $i$  and  $j$ , and the relative positions of these species in the network.

One simple prediction one might make is that species that share a direct connection in the network tend to covary more strongly than those that do not. In general, one might expect that the covariance bewteen two species tends to decrease as the network distance (i.e. length of the shortest path between them) increases. Indeed, this is broadly what we find, see Figure 10. Note that when the system is near its tipping point, it appears that covariance between nodes persists over longer network distances than when the system is far from its tipping point.

Next we look in more detail at how the dependence of covariance on network

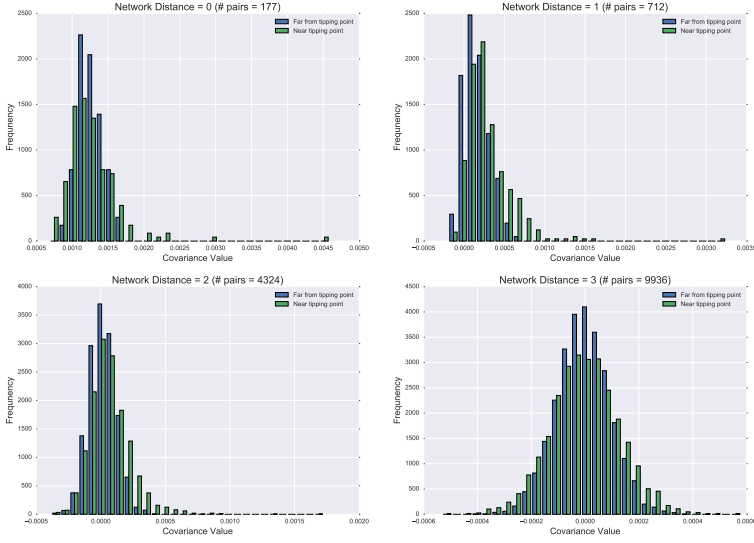


Figure 11: Histograms of covariance values, near to vs. far from the tipping point, at network distances 0, 1, 2, and 3 (network distance from  $i$  to  $j$  is 0 if and only if  $i = j$ ). In all cases the distributions of covariances appear more broad close to the tipping point, and for distances 0, 1, and 2 they also appear skewed to the right. Note the outliers in the distance-0 histogram near the tipping point, which are the variances of the species that are about to go extinct.

distance changes as the system approaches its tipping point. One way to do this is the following; for each value of network distance (starting with 0, 1, 2, 3), plot a histogram of covariances of nodes at that distance, both near to and far from the tipping point. The result is shown in Figure 11.

Another salient feature in the covariance between two species is each of their respective degrees. Consider the following: the more mutualistic partners a species has, the less susceptible it is to fluctuations in the abundance of any single one of its partners. Hence one could reasonably expect that higher-degree species covary less strongly with their neighbors than lower-degree species do. This intuition is borne out in the data, as depicted in Figure 12. This intuition can (I think) be made precise by an application of the central limit theorem, by interpreting the mutualistic benefit obtained by a species as a sample average of its neighbors' randomly fluctuating abundances.

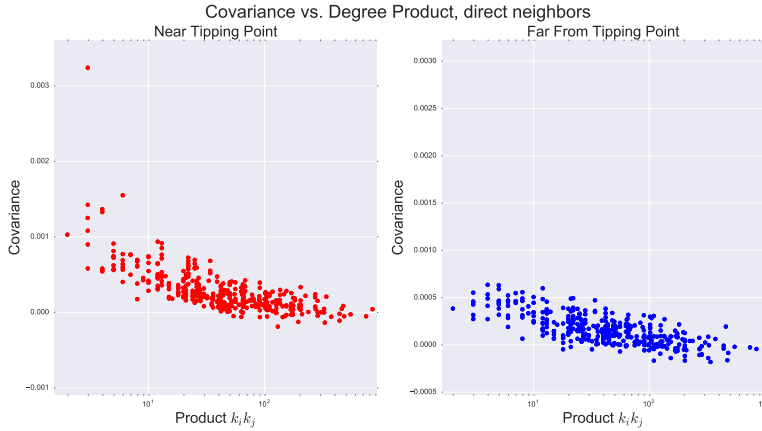


Figure 12: Covariance between direct neighbors as a function of the product of their degrees. Generalist species that interact with other generalist species covary weakly, as indicated by the downward trend. Data are plotted on a semi-log plot, indicating a roughly-linear dependence of  $\text{Cov}(i, j)$  on  $\log(k_i) + \log(k_j)$ .

## 12 Randomizing the Network

Now we report observations of the dynamics on a randomized version of the original network. We randomize the network by performing a link-swapping procedure that ensures the degree of each node remains fixed and that there are no repeated edges or self-loops.

Figure 13 shows an overview of the unfolding of community collapse in the original network and the randomized network. One notable feature is that in the randomized network, there seem to be fewer abrupt shifts, either up or down, of species abundance as a function of population.

To look in more detail at the difference between these two cases, we construct a histogram of "times" at which species went extinct, Figure 14. In the present context, "time" progresses in integer steps from 0 to 200, with each step corresponding to a decrease in  $\gamma_0$  of size 8/200 (so that  $\gamma_0$  goes from 8 to 0 after 200 time steps). The horizontal axis in Figure 14 is simply a reversed and rescaled version of that in Figure 13.

## 13 Varying Nestedness

Here we report results of simulations performed on a family of networks, alike in shape (number of plants and number of animals), number of links, and expected degree distribution, but varying in nestedness. To do this we used an algorithm adapted from [?] (SI).

Intuitively, the network structure linking species together should have an effect on their overall ability to survive. One may expect [Cai, personal com-

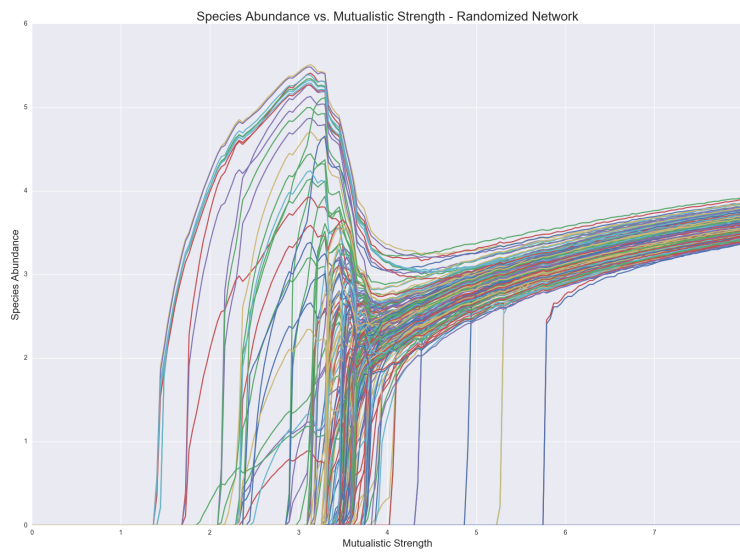
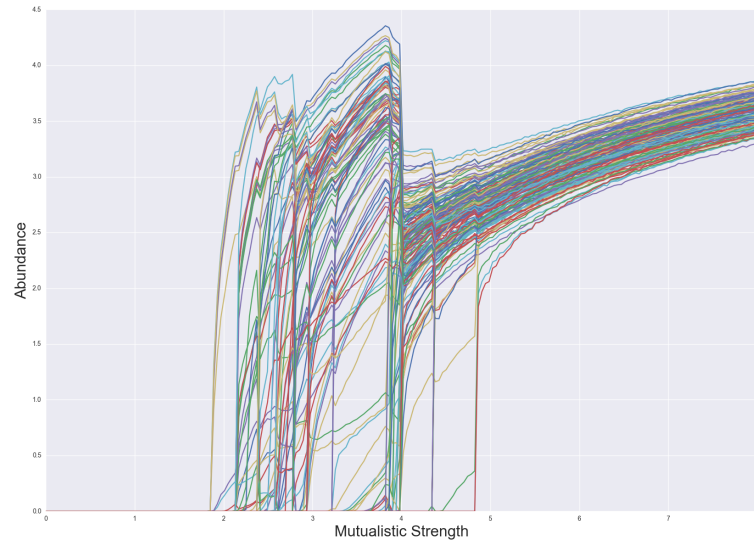


Figure 13: Overall ecosystem collapse on the original network vs. the randomized network.

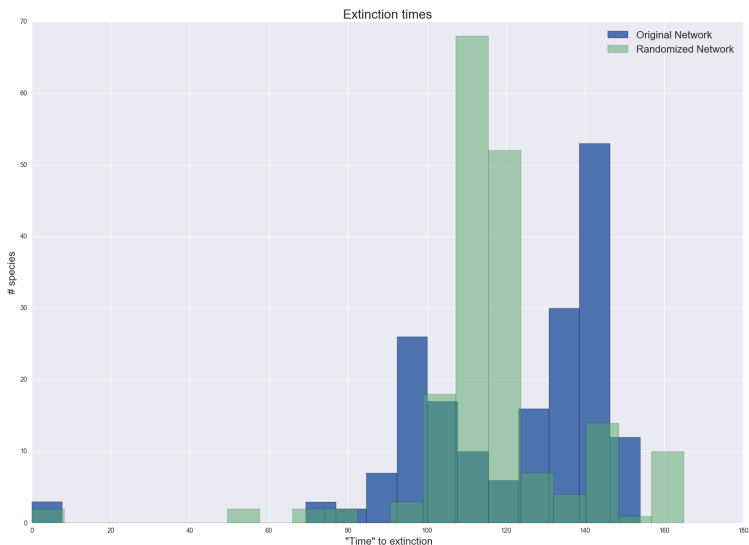


Figure 14: Histogram of times at which species went extinct on the original network (blue) and on the randomized network (translucent green). Note that in the original network there appear to be two groups of extinctions, possibly aligning with a modular structure of the network.

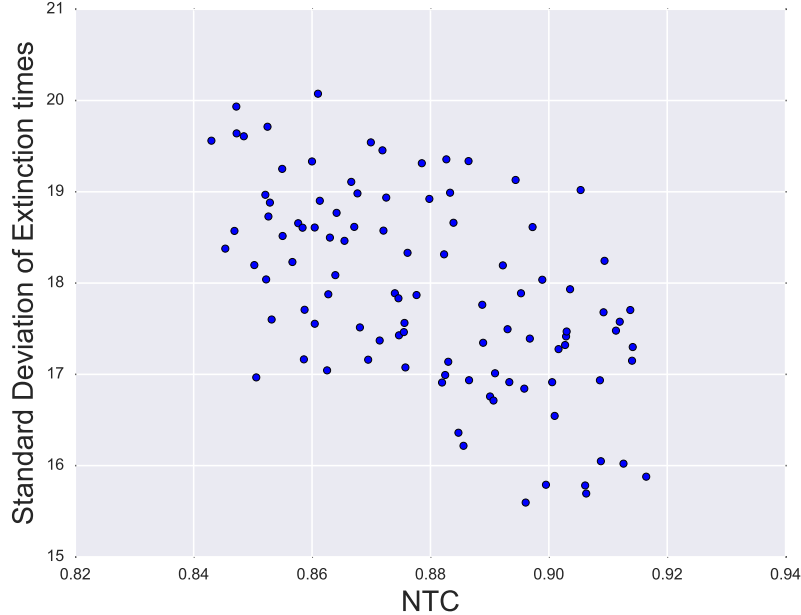


Figure 15: Standard deviation of extinction times, plotted against nestedness. Note the (very noisy) downward trend, indicating that with greater nestedness comes tighter bunching of extinction events.

munication] that in a highly nested network, species may tend to go extinct together more so than in a less nested network. To check this, we simply compute the standard deviation of the times at which species go extinct, and plot this against nestedness Figure 15. However, other measures such as the difference between the first and last extinction event, the size of the first extinction event, and the size of the largest extinction event, do not appear to show any trend with NTC, and we do not show plots of them.

## 14 Histogramology

Following [BB13], we consider distributions of covariance (and correlation) values. In [BB13], the authors outline general considerations for a wide class of dynamics on networks (a class that, unfortunately, does not contain our model) that show that one should expect the correlations among system variables to be distributed according to a power law - and moreover, that the exponent of this power law can be derived from properties of the functions defining the network dynamics at hand. Similar arguments establish expected power-law distributions in other quantities related to influence, susceptibility, and spreading of

perturbations.

Since, as mentioned, our model does not fall properly in the class considered by [BB13], we cannot directly apply their method to compute what we should expect our power-law exponents to be. We can, however, simply measure them!

I should state a strong caveat here: [BB13] considers *correlations*, which (they claim) is equivalent to a matrix of derivatives  $G_{ij} = |dx_i/dx_j|$ , where the derivative is taken to measure the effect of the fixed-point value of variable  $x_i$  in response to an imposed perturbation on  $x_j$ . However, we've found the most interesting and interpretable things in looking at *covariances* rather than correlations.

An illustrative example is given in Figure 16. This figure shows histograms in a log scale, and so straight lines correspond to power-law behavior. In these figures, data are grouped in linear-sized bins, hence their unequal widths on the log scale.

For both the low and high nestedness networks, we see an understandable difference in the distribution of covariance values near the tipping point vs. far from it. When the system is far from the tipping point, we see a hump in the right side of the distribution - this consists (it turns out) of the diagonal entries of the covariance matrix. That is, these are the variances of the individual system variables, and all the off-diagonal entries (i.e. the covariances) are smaller in magnitude.

The situation changes, however, as the system approaches its tipping point - the distribution of covariance values appears to be approximately a single power-law, indicating that covariance values have increased to the point of being comparable with variances. At this point, we do not have a quantification of this in a precise enough way to talk about a trend with respect to nestedness, or the robustness of this phenomenon across network instances.

Note that this result is consistent with what was shown in Figure 10, though at a coarser level of detail. Figure 10 shows side-by-side box plots indicating the spread of covariance values at various network distances - in the far-from-tipping-point case, the distance-zero data points are well-separated from the rest of the points, while in the near-tipping point case, distance-one covariances are comparable to distance-zero covariances.

## 15 Analytical Results

Here we report calculations that illuminate the behavior of Equation 2 in various special cases

### 15.1 Zero interspecies competition, $\delta = 1$

As mentioned in subsection 8.2, the dynamics are very simple in the case of zero competition and  $\delta = 1$ . Upon examination of Figure 2, it is reasonable to guess that for any given value of  $\gamma_0$ , the system has a fixed point in which all species abundances are nearly equal.

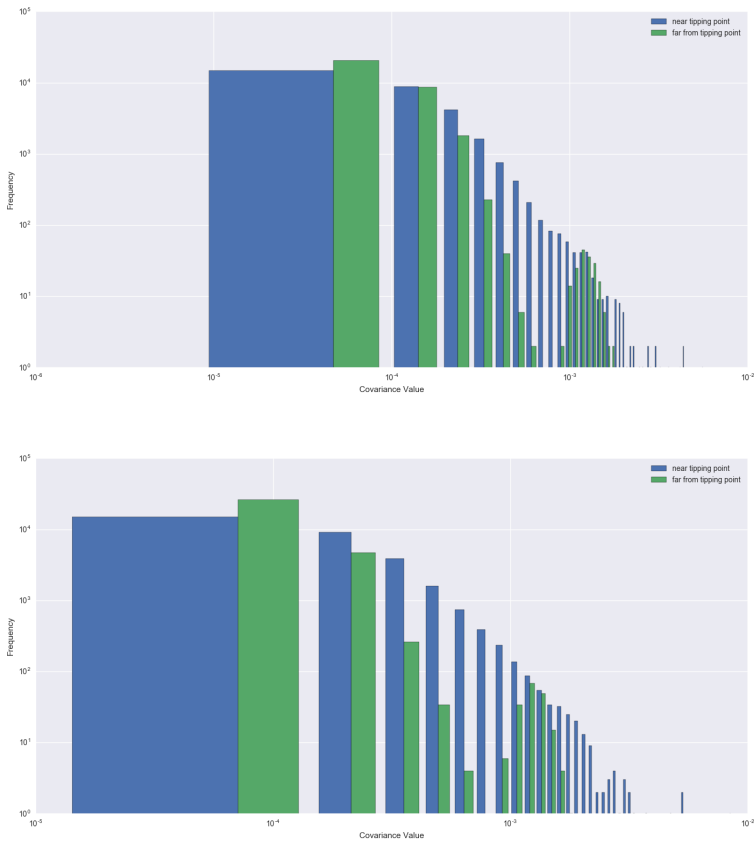


Figure 16: Histograms of covariance values, near the tipping point (blue) vs. far from the tipping point (green). Upper panel is a network with low nestedness, lower panel is a network with high nestedness.

Indeed, if we have  $P_i = \bar{P}$  and  $A_j = \bar{A}$  for all  $i, j$ , then the mutualistic terms become

$$\sum_{j=1}^{N_A} \gamma_{ij}^P A_j = \sum_{j=1}^{N_A} \gamma_0 \frac{y_{ij}}{k_i} \bar{A} = \gamma_0 \bar{A} \quad (47)$$

and so it is possible to write closed evolution equations for the quantities  $\bar{P}, \bar{A}$ . Averaging the equations for  $dP_i/dt$  and  $dA_j/dt$  over  $i$  and  $j$ , respectively, gives

$$\frac{d\bar{A}}{dt} = \bar{A} \left( \bar{\alpha}^A - \bar{A} + \frac{\gamma_0 \bar{P}}{1 + h\gamma_0 \bar{P}} \right) \quad (48)$$

$$\frac{d\bar{P}}{dt} = \bar{P} \left( \bar{\alpha}^P - \bar{P} + \frac{\gamma_0 \bar{A}}{1 + h\gamma_0 \bar{A}} \right) \quad (49)$$

where  $\bar{\alpha}^P = \sum_i \alpha_i^P / N_P$ , and similarly for  $\bar{\alpha}^A$ . For the numerical values chosen in the simulations described above,  $\bar{\alpha}^A = \bar{\alpha}^P = a = -0.3$ .

Due to the symmetry of these equations, we suppose that there is a fixed point solution with  $\bar{A} = \bar{P} = x > 0$ , and find that this is true if

$$h\gamma_0 x^2 + (1 - \gamma_0(1 + ah))x + a = 0. \quad (50)$$

This quadratic equation has either two, one, or zero solutions for  $x$ , depending on the sign of the discriminant. The discriminant changes sign when

$$(1 - \gamma_0(1 + ah))^2 + 4ah\gamma_0 = 0 \quad (51)$$

which is now a quadratic equation for  $\gamma_0$ . We find that the discriminant changes sign when

$$\gamma_0 = \frac{1 - ah \pm 2\sqrt{-ah}}{(1 + ah)^2}. \quad (52)$$

Using the numerical values of  $a = -0.3$  and  $h = 0.1$ , we find  $\gamma_0 = 0.73, 1.46$ , the latter of which coincides closely with the onset of total ecosystem collapse in the second part of Figure 2.

We can in fact compute the relevant solution to Equation 50, and plot it alongside the simulation results. The result is shown in Figure 17.

## 15.2 Uniform Growth Rate

Here we report results about the system Equation 2 in the case where 1)  $\alpha_i = \alpha$  for all  $i$ , 2)  $\delta = 1$ , and 3)  $\beta_{ij}^G = \varepsilon/(N_G - 1)$  for  $i \neq j$ ,  $\beta_{ii}^G = 1$ ,  $G \in \{A, P\}$ . This is effectively the same situation as discussed in subsection 15.1 except that we allow weak competition (whose strength is governed by the small parameter  $\varepsilon$ ). What we will demonstrate is that the competition matrix has a strong effect on the nature of the extinction process on a mutualistic network.

Under these assumptions, there is effectively no difference between any two species, and so there is a fixed point solution in which all species abundances

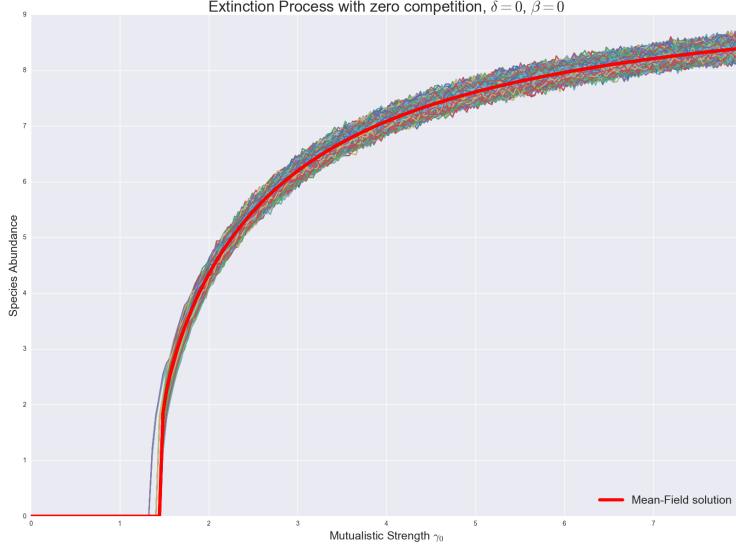


Figure 17: Simulation results together with mean-field solution. Note excellent agreement.

are equal. This common value,  $x$ , of abundance satisfies a quadratic equation with the other parameters of the model:

$$0 = \alpha - (1 + \varepsilon)x + \frac{\gamma_0 x}{1 + h\gamma_0 x} \quad (53)$$

$$0 = -h\gamma_0(1 + \varepsilon)x^2 + (\gamma_0(1 + ah) - (1 + \varepsilon))x + \alpha \quad (54)$$

Applying the quadratic formula, we get

$$x = \frac{1 + \varepsilon - \gamma_0(1 + ah) \pm \sqrt{(\gamma_0(1 + ah) - (1 + \varepsilon))^2 + 4\alpha h\gamma_0(1 + \varepsilon)}}{-2h\gamma_0(1 + \varepsilon)} \quad (55)$$

Treating all parameters as constant except for  $\gamma_0$ , we see that there are either 2, 1, or 0 solutions for  $x$ , depending on the sign of the discriminant. The discriminant is a concave-up quadratic function of  $\gamma_0$ , which means that for large enough  $\gamma_0$ , the discriminant is positive and there are two solutions for  $x$ . These solutions  $x^\pm$  meet and annihilate at the value of  $\gamma_0$  that makes the discriminant zero, i.e. the solutions to the equation

$$0 = \gamma_0^2(1 + h\alpha)^2 + 2\gamma_0(h\alpha - 1)(1 + \varepsilon) + (1 + \varepsilon)^2 \quad (56)$$

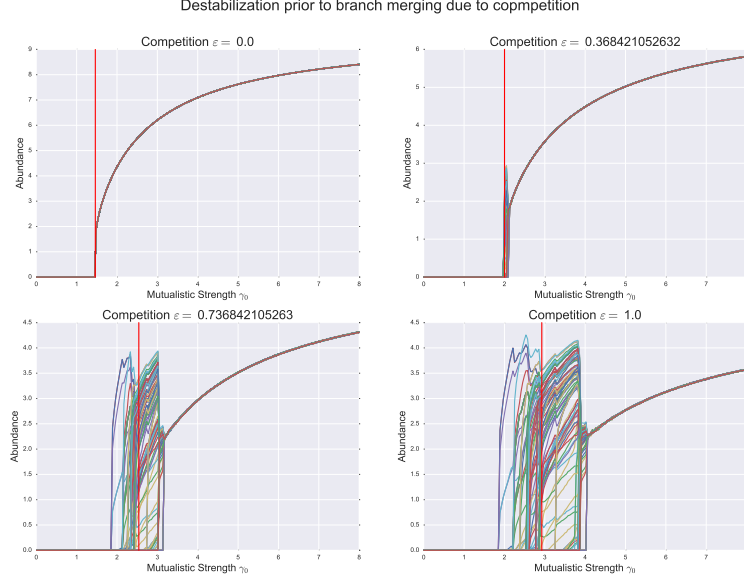


Figure 18: Depiction of the effect of competition on the stability of the state in which all abundances are equal. Irrespective of  $\varepsilon$ , there are two branches of solutions in which all species have equal abundance, and they merge at a value of  $\gamma_0$  indicated by the vertical red line. However, for  $\varepsilon > 0$ , the upper branch becomes unstable before it meets the lower branch, contrary to a typical saddle-node bifurcation.

which are

$$\gamma_0 = (1 + \varepsilon) \left[ \frac{1 - \alpha h \pm 2\sqrt{-\alpha h}}{(1 + \alpha h)^2} \right] = (1 + \varepsilon) \left( \frac{1 \pm \sqrt{-\alpha h}}{1 + \alpha h} \right)^2 \quad (57)$$

At this point, the situation resembles a standard saddle-node bifurcation. However we will show that it is not always true that one branch is stable and the other is unstable up until their meeting point. Indeed, the stability of this fixed point is governed by the largest (real part of an) eigenvalue of the Jacobian, which in this case is (in block form)

$$J = \left[ \begin{array}{c|c} x\beta^P & \frac{\gamma_0 x}{1+h\gamma_0 x} \Gamma^{P \leftarrow A} \\ \hline \frac{\gamma_0 x}{1+h\gamma_0 x} \Gamma^{A \leftarrow P} & x\beta^A \end{array} \right] \quad (58)$$

where  $\Gamma_{ij}^{P \leftarrow A} = y_{ij}/k_i$ . At this state we don't have analytical results on the spectrum of  $J$  as a function of  $\varepsilon$  and  $\gamma_0$ , but we do have numerical evidence that an eigenvalue of  $J$  crosses the imaginary axis at a value of  $\gamma_0$  *greater* than the value at which the two branches meet. The situation is depicted in Figure 18.

This result indicates that the competition matrix has a strong effect on the spectral properties of the Jacobian, and hence on the early warning signals one should expect prior to a tipping point. This is philosophically aligned with recent work such as [GLHBHM17], which establishes that dependencies between the competitive network and the mutualistic network have a nontrivial impact on the carrying capacity of a mutualistic ecosystem.

## Part IV

# Reframing

Here I'm going to describe some ways to reframe the project at hand.

What we really wanted to get at all along was the connection between the topology of mutualistic networks and the dynamics of spreading processes on them, such as cascading extinction events. We thought that we could get some insights into this at the level of SDE models; that line of inquiry hasn't produced the sort of insight we were looking for.

Instead, we'll study highly simplified model of spreading process on simplified networks. In particular, we choose the Watts threshold model, because it is very simple and captures certain salient features of extinction cascades: that an extinction occurs when a species loses too many of its partners.

## 16 Random network models

For the networks on which to study a threshold spreading model, we consider primarily two models, both designed to produce networks that are simultaneously nested and modular.

First is a model described in [?], based on previous work in [GN05], [OH08], and [SRG07]. The model depends primarily on two free parameters,  $p_{\text{comp}}$  and  $p_{\text{nest}}$ , determining the extent of modularity and nestedness, respectively. Specification of the model also requires specifying a *partition* of the nodes of each guild, and a level of *connectance* (i.e. fraction of possible links that are present).

The sampling algorithm is as follows:

Let  $N_A$  and  $N_P$  be the number of animal and plant species, respectively. For each animal (plant) species  $i$  ( $j$ ), draw a sample from a power-law distribution with exponent (say) -2,  $P_i^A$  ( $P_j^P$ ). This number will represent that node's *expected degree*.

Given the desired connectance  $C$ , let  $N_L = \lfloor CN_A N_P \rfloor$  be the total number of links. While total number of links is less than  $N_L$ , do the following:

1. With probability  $p_{\text{nest}}$ , choose an animal species  $i$  with probability proportional to  $P_i^A$ . With probability  $1 - p_{\text{nest}}$ , choose an animal species  $i$  with uniform probability (i.e. probability  $1/N_A$ ).
2. With probability  $p_{\text{comp}}$ , choose a plant species  $j$  from the same module as animal species  $i$ . With probability  $1 - p_{\text{comp}}$ , choose a plant species from among all plant species.
3. With probability  $p_{\text{nest}}$ , choose  $j$  with probability proportional to  $P_j^P$ , and with probability  $1 - p_{\text{nest}}$ , choose  $j$  with uniform probability.
4. Add a link between nodes  $i$  and  $j$  if one does not already exist. Otherwise, do nothing.

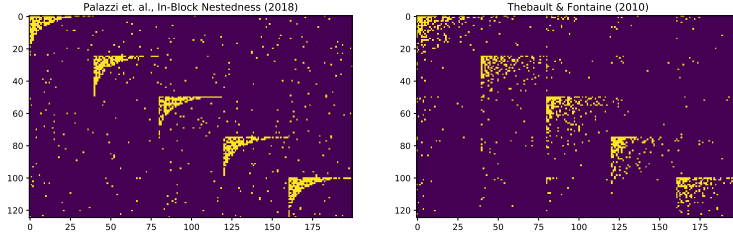


Figure 19: Comparison of the random network models described in [PBHTSR18] (left) and [TF10] (right). Both networks have the same number of modules with the same shapes, the same total number of links, and the same fraction of links within modules vs. between modules.

To account for possible asymmetry due to the order of selecting nodes, do the above procedure with probability 1/2 and do the opposite (i.e. interchange plant and animal guilds) with probability 1/2.

Another method is described in [PBHTSR18], and is designed to produce network structures that are modular and nested. See their text for a full description: a sample using their method is shown in Figure 19.

## 17 Dynamics

Now we describe the dynamics that we put on the networks defined above.

Let  $N$  be the total number of nodes in a network and let  $A \in \{0, 1\}^{N \times N}$  denote its adjacency matrix:  $A_{ij} = 1$  if and only if nodes  $i$  and  $j$  share an edge, and we assume all edges are undirected and unweighted. Let  $k_i = \sum_j A_{ij}$  denote the degree of node  $i$ .

Let  $u \in \{0, 1\}^N$  denote the *state* of the system;  $u_i = 1$  if species  $i$  is present, and zero otherwise. We introduce a dynamic on  $u$  according to the rule

$$u_i(t+1) = \begin{cases} 1 & \sum_j A_{ij} u_j(t) > \theta k_i \text{ and } u_j(t) = 1 \\ 0 & \text{else} \end{cases} \quad (59)$$

where  $\theta \in [0, 1]$  is the *threshold*. In words, a species can only survive if at least some critical fraction of its mutualistic partner species are present. Note that in general  $\theta$  could be different for each species, but we assume here that it is the same.

This dynamic can happen on any network; in our setting we are interested in the case when it is bipartite, and shows a nested and modular structure.

The dynamics are as follows. Let  $u \in \{0, 1\}^N$

## References

- [ANGLU08] Mário Almeida-Neto, Paulo R. Guimarães, Rafael D. Loyola, and Werner Ulrich. A consistent metric for nestedness analysis in ecological systems: reconciling concept and measurement. *Oikos*, 117(8):1227–1239, aug 2008.
- [AP93] W Atmar and B D Patterson. The measure of order and disorder in the distribution of species in fragmental habitat. *Oecologia*, 96:373–382, 1993.
- [Bar07] Michael J. Barber. Modularity and community detection in bipartite networks. *Physical Review E - Statistical, Nonlinear, and Soft Matter Physics*, 76(6):1–9, 2007.
- [Bar14] Paolo Barucca. Localization in covariance matrices of coupled heterogenous Ornstein-Uhlenbeck processes. *Physical Review E - Statistical, Nonlinear, and Soft Matter Physics*, 90(6):1–5, 2014.
- [BB13] Baruch Barzel and Albert-László Barabási. Universality in network dynamics. *Nature physics*, 9(10):673–681, 2013.
- [BFPG<sup>+</sup>09] Ugo Bastolla, Miguel A. Fortuna, Alberto Pascual-García, Antonio Ferrera, Bartolo Luque, and Jordi Bascompte. The architecture of mutualistic networks minimizes competition and increases biodiversity. *Nature*, 458(7241):1018–1020, 2009.
- [BJMO03] Jordi Bascompte, P. Jordano, C. J. Melian, and Jens M. Olesen. The nested assembly of plant-animal mutualistic networks. *Proceedings of the National Academy of Sciences*, 100(16):9383–9387, 2003.
- [DB14] Vasilis Dakos and Jordi Bascompte. Critical slowing down as early warning for the onset of collapse in mutualistic communities. *Proceedings of the National Academy of Sciences*, 111(49):17546–17551, 2014.
- [Gar96] Crispin W. Gardiner. Handbook of stochastic methods: For Physics, Chemistry and the Natural Sciences, 1996.
- [GLHBHM17] Carlos Gracia-Lázaro, Laura Hernández, Javier Borge-Holthoefer, and Yamir Moreno. The joint influence of competition and mutualism on the biodiversity of mutualistic ecosystems. pages 1–11, mar 2017.
- [GN05] Roger Guimerà and Luís A. Nunes Amaral. Functional cartography of complex metabolic networks. *Nature*, 433(7028):895–900, feb 2005.

- [GRA16] Jacopo Grilli, Tim Rogers, and Stefano Allesina. Modularity and stability in ecological communities. *Nature Communications*, 7(May):1–10, 2016.
- [MG13] Mel MacMahon and Diego Garlaschelli. Community detection for correlation matrices. pages 1–35, 2013.
- [New06] Mark Newman. Modularity and community structure in networks. *Proceedings of the National Academy of Sciences*, 103(23):8577–8582, 2006.
- [OBDJ07] Jens M. Olesen, Jordi Bascompte, Y. L. Dupont, and P. Jordano. The modularity of pollination networks. *Proceedings of the National Academy of Sciences*, 104(50):19891–19896, 2007.
- [OH08] Toshinori Okuyama and J. Nathaniel Holland. Network structural properties mediate the stability of mutualistic communities. *Ecology Letters*, 11(3):208–216, 2008.
- [PBHTSR18] María Palazzi, Javier Borge-Holthoefer, Claudio Tessone, and Albert Solé-Ribalta. Antagonistic Structural Patterns in Complex Networks. *arXiv Social and Information Networks*, oct 2018.
- [PHM17] Claudia Payrato Borras, Laura Hernandez, and Yamir Moreno. Breaking the spell of nestedness. *bioRxiv*, pages 1–8, jan 2017.
- [SBB<sup>+</sup>09] Marten Scheffer, Jordi Bascompte, William A. Brock, Victor Brovkin, Stephen R. Carpenter, Vasilis Dakos, Hermann Held, Egbert H. Van Nes, Max Rietkerk, and George Sugihara. Early-warning signals for critical transitions. *Nature*, 461(7260):53–59, 2009.
- [SD14] Samir Suweis and Paolo D’Odorico. Early warning signs in social-ecological networks. *PLoS ONE*, 9(7), 2014.
- [SRG07] Luis Santamaría and Miguel A Rodríguez-Gironés. Linkage Rules for PlantPollinator Networks: Trait Complementarity or Exploitation Barriers? *PLoS Biology*, 5(2):e31, jan 2007.
- [SRTU09] Serguei Saavedra, Felix Reed-Tsochas, and Brian Uzzi. A simple model of bipartite cooperation for ecological and organizational networks. *Nature*, 457(7228):463–466, 2009.
- [TF10] E. Thebault and Colin Fontaine. Stability of Ecological Communities and the Architecture of Mutualistic and Trophic Networks. *Science*, 329(5993):853–856, aug 2010.